

# Binary black holes in the pair-instability mass gap

Ugo N. Di Carlo<sup>1,2,3</sup>, Michela Mapelli<sup>4,2,3</sup>, Yann Bouffanais<sup>4,2</sup>, Nicola Giacobbo<sup>4,2,3</sup>, Filippo Santoliquido<sup>4,2</sup>, Alessandro Bressan<sup>5</sup>, Mario Spera<sup>2,4,6,7</sup> and Francesco Haardt<sup>1</sup>

<sup>1</sup>*Dipartimento di Scienza e Alta Tecnologia, University of Insubria, Via Valleggio 11, I-22100, Como, Italy*

<sup>2</sup>*INFN, Sezione di Padova, Via Marzolo 8, I-35131, Padova, Italy*

<sup>3</sup>*INAF-Osservatorio Astronomico di Padova, Vicolo dell'Osservatorio 5, I-35122, Padova, Italy*

<sup>4</sup>*Dipartimento di Fisica e Astronomia 'G. Galilei', University of Padova, Vicolo dell'Osservatorio 3, I-35122, Padova, Italy*

<sup>5</sup>*Scuola Internazionale Superiore di Studi Avanzati (SISSA), Via Bonomea 265, I-34136 Trieste, Italy*

<sup>6</sup>*Center for Interdisciplinary Exploration and Research in Astrophysics (CIERA), Evanston, IL 60208, USA*

<sup>7</sup>*Department of Physics & Astronomy, Northwestern University, Evanston, IL 60208, USA*

7 July 2020

## ABSTRACT

Pair instability (PI) and pulsational PI prevent the formation of black holes (BHs) with mass  $\gtrsim 60 M_{\odot}$  from single star evolution. Here, we investigate the possibility that BHs with mass in the PI gap form via stellar mergers and multiple stellar mergers, facilitated by dynamical encounters in young star clusters. We analyze  $10^4$  simulations, run with the direct N-body code NBODY6++GPU coupled with the population synthesis code MOBSE. We find that up to  $\sim 6\%$  of all simulated BHs have mass in the PI gap, depending on progenitor's metallicity. This formation channel is strongly suppressed in metal-rich ( $Z = 0.02$ ) star clusters, because of stellar winds. BHs with mass in the PI gap are initially single BHs but can efficiently acquire companions through dynamical exchanges. We find that  $\sim 21\%$ ,  $10\%$  and  $0.5\%$  of all binary BHs have at least one component in the PI mass gap at metallicity  $Z = 0.0002$ ,  $0.002$  and  $0.02$ , respectively. Based on the evolution of the cosmic star formation rate and metallicity, and under the assumption that all stars form in young star clusters, we predict that  $\sim 5\%$  of all binary BH mergers detectable by advanced LIGO and Virgo at their design sensitivity have at least one component in the PI mass gap.

**Key words:** black hole physics – gravitational waves – methods: numerical – galaxies: star clusters: general – stars: kinematics and dynamics – binaries: general

## 1 INTRODUCTION

The mass function of stellar black holes (BHs) is highly uncertain, as it crucially depends on complex physical processes affecting the evolution and the final fate of massive stars. For a long time, we had to rely on a scanty set of observational data, mostly dynamical mass measurements of compact objects in X-ray binaries (Özel et al. 2010; Farr et al. 2011). In the last four years, gravitational wave (GW) data have completely revolutionised our perspective: ten binary black holes (BBHs) have been observed during the first and the second observing run of the LIGO-Virgo collaboration (LVC; Abbott et al. 2016b; Abbott et al. 2016a, 2019a,b) and we expect that several tens of new BBH mergers will be available as a result of the third observing run. GW data will soon provide a Rosetta Stone to decipher the mass function of BBHs.

Thus, it is particularly important to advance our theoretical understanding of BH formation and BH mass func-

tion, in order to provide an interpretative key for future GW data. We currently believe that the mass of a BH depends mainly on the final mass of its progenitor star and on the details of the supernova (SN) explosion (e.g. Heger et al. 2003; Mapelli et al. 2009, 2010, 2013; Belczynski et al. 2010; Fryer et al. 2012; Spera et al. 2015; Limongi & Chieffi 2018). Among all types of SN explosion, pair instability SNe (PISNe) and pulsational pair instability SNe (PPISNe) are expected to leave a strong fingerprint on the mass function of BHs. If the He core mass is larger than  $\sim 30 M_{\odot}$ , soon after carbon burning when the stellar core temperature reaches  $\sim 7 \times 10^8$  K, effective pair production softens the equation of state, leading to a loss of pressure. The stellar core contracts, triggering neon, oxygen and even silicon burning in a catastrophic way, known as pair instability (PI). Stars developing a helium core mass  $64 \leq m_{\text{He}}/M_{\odot} \leq 135$  are thought to be completely disrupted by a PISN, leaving no compact object (Heger et al. 2003). Stars with a smaller helium core ( $32 \lesssim m_{\text{He}}/M_{\odot} \lesssim 64$ ) undergo pulsational PI:

they go through a series of pulsations, losing mass with an enhanced rate, till their cores leave the mass range for PI (Woosley et al. 2007).

The combination of PISNe and PPISNe leads to a mass gap in the BH mass function between  $\sim 60 M_{\odot}$  and  $\sim 120 M_{\odot}$ . Both the lower and the upper edge of the mass gap depend on the details of massive star evolution. In particular, the lower edge of the mass gap might span from  $\sim 40 M_{\odot}$  up to  $\sim 65 M_{\odot}$ , depending on the details of PI, stellar evolution and core-collapse SNe (Belczynski et al. 2016; Woosley 2017, 2019; Spera & Mapelli 2017; Giacobbo et al. 2018; Giacobbo & Mapelli 2018; Marchant et al. 2019; Mapelli et al. 2020; Stevenson et al. 2019; Farmer et al. 2019; Renzo et al. 2020). The upper edge of the gap is even more uncertain. LIGO-Virgo data from the first and second observing run are consistent with a maximum BH mass of  $\approx 45 M_{\odot}$ , in agreement with the existence of a PI mass gap (Abbott et al. 2019b).

However, some exotic BH formation channels might populate the PI gap. Hence, the detection of a BH in the mass gap by the LVC would possibly provide a smoking gun for these exotic channels. Primordial BHs (i.e. BHs formed from the collapse of gravitational instabilities in the early Universe, e.g. Carr & Hawking 1974; Carr et al. 2016) might have a mass in the gap. Alternatively, BHs with mass in the gap can form as “second-generation” BHs (Gerosa & Berti 2017), i.e. BHs born from the merger of two smaller BHs.

Finally, Spera et al. (2019) and Di Carlo et al. (2019) proposed a third possible channel to produce BHs in the mass gap. If a massive star with a well-developed helium core merges with a non-evolved companion (a main sequence or an Hertzsprung-gap star), it might give birth to an evolved star with an over-sized hydrogen envelope. If the helium core remains below  $\sim 32 M_{\odot}$  and the star collapses to a BH before growing a much larger core and before losing a significant fraction of its envelope, the final BH might be in the PI mass gap.

If a second-generation BH or a BH born from stellar merger form in the field, they remain single objects and we do not expect to observe them in a BBH merger. In contrast, if they form in a dense stellar cluster they might capture a new companion through a dynamical exchange, possibly becoming a BBH (Miller & Hamilton 2002; Di Carlo et al. 2019; Rodriguez et al. 2019; Gerosa & Berti 2019). Here, we focus on BHs in the PI gap formed from stellar mergers and we estimate their mass range, merger efficiency and detection probability.

## 2 METHODS

The simulations discussed in this paper were done using the same code and methodology as described in Di Carlo et al. (2019). In particular, we use the direct summation N-Body code NBODY6++GPU (Wang et al. 2015) coupled with the new population synthesis code MOBSE (Mapelli et al. 2017; Giacobbo et al. 2018; Giacobbo & Mapelli 2018). MOBSE includes up-to-date prescriptions for massive star winds, for core-collapse SN explosions and for PISNe and PPISNe.

In this work, we have analyzed the simulations of  $10^4$  fractal young star clusters (SCs); 4000 of them are the simulations presented in Di Carlo et al. (2019), while the re-

maining 6000 are discussed in Di Carlo et al. (2020). The initial conditions of the simulations presented in this paper are summarized in Table 1. Unlike globular clusters, young SCs are asymmetric, clumpy systems. Thus, we model them with fractal initial conditions (Küpper et al. 2011), to mimic initial clumpiness (Goodwin & Whitworth 2004). The level of fractality is decided by the parameter  $D$  (where  $D = 3$  means homogeneous distribution of stars). In this work, we assume  $D = 1.6, 2.3$ .

The total mass  $M_{\text{SC}}$  of each SC (ranging from  $10^3 M_{\odot}$  to  $3 \times 10^4 M_{\odot}$ ) is drawn from a distribution  $dN/dM_{\text{SC}} \propto M_{\text{SC}}^{-2}$ , as the embedded SC mass function described in Lada & Lada (2003). We choose to simulate SCs with mass  $M_{\text{SC}} < 30000 M_{\odot}$  for computational reasons. Thus, the mass distribution of our simulated SCs mimics the mass distribution of SCs in Milky Way-like galaxies. We choose the initial SC half mass radius  $r_{\text{h}}$  according to the Marks & Kroupa relation (Marks et al. 2012) in 7000 simulations, and we adopt a fix value  $r_{\text{h}} = 1.5$  pc for the remaining 3000 simulations.

The stars in the simulated SCs follow a Kroupa (2001) initial mass function, with minimum mass  $0.1 M_{\odot}$  and maximum mass  $150 M_{\odot}$ . We assume an initial binary fraction  $f_{\text{bin}} = 0.4$ . The orbital periods, eccentricities and mass ratios of binaries are drawn from Sana et al. (2012). We simulate each star cluster for 100 Myr in a rigid tidal field corresponding to the Milky Way tidal field at the orbit of the Sun. We refer to Di Carlo et al. (2019) for further details on the code and on the initial conditions.

We consider three different metallicities:  $Z = 0.0002, 0.002$  and  $0.02$  (approximately  $1/100, 1/10$  and  $1 Z_{\odot}$ ). We divide our simulations in three sets, corresponding to metallicity  $Z = 0.0002$  (2000 runs),  $0.002$  (6000 runs) and  $0.02$  (2000 runs). The simulations with  $Z = 0.002$  are the union of the 4000 runs presented in Di Carlo et al. (2019) and 2000 runs discussed in Di Carlo et al. (2020). The simulations with  $Z = 0.02$  and  $Z = 0.0002$  are both from Di Carlo et al. (2020). The main differences between the simulations already presented in Di Carlo et al. (2019) and the new runs from Di Carlo et al. (2020) are i) the efficiency of common envelope ejection ( $\alpha = 3$  in Di Carlo et al. 2019 and  $\alpha = 5$  in Di Carlo et al. 2020), and ii) the model of core-collapse supernova (the rapid and the delayed models from Fryer et al. 2012 are adopted in Di Carlo et al. 2019 and in Di Carlo et al. 2020, respectively). Putting together these different samples is not a completely consistent approach, but is justified by the fact that the population of BHs with mass in the  $60 - 150 M_{\odot}$  range is not strongly affected by these different assumptions. For example, in Di Carlo et al. (2020), we showed that our different assumptions change the percentage of BHs in the gap by a factor of  $\sim 1.1 - 1.5$  (this is much less than the impact of stellar metallicity we want to probe here). Finally, putting together different SC models is important to filter out stochastic fluctuations, since the formation of BHs in the gap is a rare event and our simulations are computationally expensive.

## 3 RESULTS

From our simulations, we extract information on BHs with mass in the PI gap, between  $60$  and  $150 M_{\odot}$  (given the uncertainties on the edges of the mass gap, we make a con-

**Table 1.** Initial conditions.

Set	$Z$	$N_{\text{sim}}$	$r_{\text{h}}$	$D$	ref.
Z0002	0.0002	1000	M2012	1.6	D2020
	0.0002	1000	1.5 pc	1.6	D2020
Z002	0.002	2000	M2012	2.3	D2019
	0.002	3000	M2012	1.6	D2019, D2020
	0.002	1000	1.5 pc	1.6	D2020
Z02	0.02	1000	M2012	1.6	D2020
	0.02	1000	1.5 pc	1.6	D2020

Column 1: Name of the simulation set. Column 2: metallicity  $Z$ . Column 3: Number of runs performed per each set. Column 4: half-mass radius  $r_{\text{h}}$ . M2012 indicates that half-mass radii have been drawn according to Marks et al. (2012). Column 5: fractal dimension ( $D$ ). Column 6: reference for each simulation set. D2019 and D2020 correspond to Di Carlo et al. (2019) and Di Carlo et al. (2020), respectively.

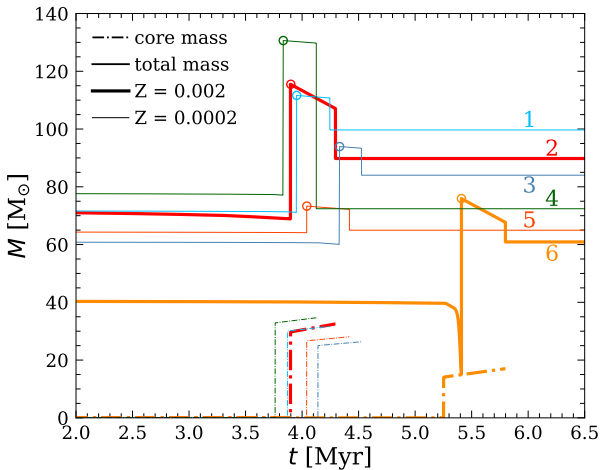


**Figure 1.** Evolution of the total mass (solid lines) and the core mass (dot-dashed lines) of the progenitors of a sample of BHs with mass in the gap. The open circle marks the time of the merger with a companion star. Thick lines:  $Z = 0.002$ ; thin lines:  $Z = 0.0002$ . Models 1, 3 and 4 (light blue, blue and green) are stars that become single BHs; models 2, 5 and 6 (red, orange and yellow) are stars which end up in merging BBHs.

servative assumption for both the lower and the upper edge of the mass gap). In Di Carlo et al. (2019), we have already discussed the properties of BHs that form from stars with  $Z = 0.002$ , have mass in the PI gap and merge with other BHs in less than a Hubble time. Here, we extend our study to other progenitor’s metallicities ( $Z = 0.02$  and  $0.0002$ ), because stellar metallicity is a crucial ingredient to understand how many BHs can form with mass in the PI gap. Moreover, we discuss the formation pathways of BHs born from stellar mergers, by looking at the core and envelope evolution of their progenitors (Figure 1). We consider all BHs that form in the PI mass gap (both single and binary BHs) and we investigate their properties. Finally, we estimate the detectability of BHs in the mass gap by LIGO and Virgo at design sensitivity.

### 3.1 Formation channels of BHs in the gap

The vast majority of BHs with mass in the PI gap that form in our simulation originates from the merger of an evolved star (with a developed helium core of mass  $\approx 15 - 30 M_{\odot}$ ) and a main sequence companion. The merger is generally triggered by dynamical perturbations. In several cases, the evolved star is the result of multiple mergers between other stars, facilitated by the dense dynamical environment. This process of multiple mergers occurring in a very short time span is known as runaway collision and was already discussed in several papers (see e.g. Portegies Zwart & McMillan 2002; Portegies Zwart et al. 2004; Giersz et al. 2015; Mapelli 2016; Gieles et al. 2018).

Figure 1 shows the evolution of six stellar progenitors of BHs in the PI mass gap. Three of these BHs become members of BBHs and merge within a Hubble time, while the other three objects leave single BHs. We find no significant difference between the formation channel of merging BHs in the PI mass gap and that of single BHs or non-merging BBHs with mass in the PI gap.

The stars shown in Figure 1 undergo a merger with a main-sequence companion in their late evolutionary stages ( $\sim 4-6$  Myr), when they are Hertzsprung gap or core helium burning stars. We assume that there is no mass loss during the merger. The merger products are not significantly rejuvenated, because they already developed a He core. They are evolved based on their mass and are subject to stellar winds, depending on their metallicity. Their final He core is  $\sim 17 - 32 M_{\odot}$  (below the PPISN/PISN gap), while their hydrogen envelope is over-sized with respect to single star evolution, because of the merger. While most stars in Figure 1 simply merge with another star without previous mass transfer episodes, star number 6 shows signature of mass transfer. This star fills its Roche lobe after leaving the main sequence and its hydrogen envelope is removed. At the end of mass transfer, it merges with its companion.

In all the simulations, the post-merger star evolves for  $t_{\text{post-merg}} = t_{\text{He}} + t_{\text{C}} + t_{\text{Ne}} + t_{\text{O}} + t_{\text{Si}} \sim t_{\text{He}}$ , where  $t_{\text{post-merg}}$  is the time remaining to collapse, while  $t_{\text{He}}$ ,  $t_{\text{C}}$ ,  $t_{\text{Ne}}$ ,  $t_{\text{O}}$  and  $t_{\text{Si}}$  are the timescale of helium, carbon, neon, oxygen and silicon burning, respectively. During  $t_{\text{post-merg}}$ , the star converts a mass  $\Delta M_{\text{He}} \sim \dot{M}_{\text{He}} t_{\text{post-merg}}$  into heavier elements, where

$$\dot{M}_{\text{He}} \lesssim 2 \times 10^{-5} M_{\odot} \text{ yr}^{-1} \left( \frac{L_{*}}{10^6 L_{\odot}} \right) \times \left( \frac{6.3 \times 10^{18} \text{ erg g}^{-1}}{\eta_{\text{CNO}}} \right) \left( \frac{0.5}{X} \right). \quad (1)$$

In equation 1,  $L_{*}$  is the stellar luminosity,  $X$  is the hydrogen fraction and  $\eta_{\text{CNO}}$  is the efficiency of mass-to-energy conversion during the CNO cycle (e.g. Prialnik 2000).

If the final mass of the helium core  $M_{\text{He},f} = M_{\text{He}} + \Delta M_{\text{He}} < 32 M_{\odot}$ , where  $M_{\text{He}}$  is the mass of the helium core before the last stellar merger, then the star with an oversized hydrogen envelope can avoid PI and directly collapses to a BH, possibly with mass  $> 60 M_{\odot}$ . This is just an order of magnitude estimation, more refined calculations would require a hydrodynamical simulation to follow the merger (see e.g. Gaburov et al. 2010) and a stellar-evolution code to integrate nuclear burning and stellar evolution.

Once they form, BHs with mass in the gap are efficient in acquiring companions:  $\sim 21\%$  and  $\sim 10\%$  of all BBHs

have at least one member with mass in the PISN gap at  $Z = 0.0002$  and  $Z = 0.002$ , respectively. This is expected, because these BHs are significantly more massive than the other BHs and stars in the SCs, and dynamical exchanges favour the formation of more massive binaries, which are more energetically stable (see e.g. Hills & Fullerton 1980).

If we consider only BBHs merging within a Hubble time (14 Gyr) due to GW emission, only  $\sim 2.2\%$  and  $\sim 2.1\%$  of them have at least one BH in the PI gap at  $Z = 0.0002$  and  $Z = 0.002$ , respectively. We find only 11 merging BBHs with a BH in the PI gap, hence these percentages are affected by stochastic fluctuations (see Table 2 for an estimate of the uncertainties). These BBHs merge after being ejected from their parent young SC. Finally, we find no merging BBHs with members in the PI gap at solar metallicity.

None of the BBHs in our simulations hosts a second-generation BH (i.e. a BH that forms from the merger of two BHs). The low escape velocity from our SCs (up to few  $\text{km s}^{-1}$  in the most massive SCs) prevents second-generation BHs from remaining inside the cluster: all of them are ejected and cannot acquire a new companion. In contrast, in massive SCs (like globular clusters and nuclear star clusters) second-generation BHs have a significantly higher chance of remaining inside their parent cluster and acquiring a companion (see e.g. Miller & Hamilton 2002; Colpi et al. 2003; Antonini & Rasio 2016; Rodriguez et al. 2019; Arca Sedda & Benacquista 2019; Arca Sedda et al. 2020).

It is important to highlight several caveats inherent with our analysis. First, MOBSE assumes that no mass is lost during the merger while hydrodynamical simulations have shown that mass ejecta can represent up to  $\sim 25\%$  of the total mass (Gaburov et al. 2010, see also Dale & Davies 2006; Justham et al. 2014; Vigna-Gómez et al. 2019; Wu et al. 2020). We have re-simulated the six objects in Figure 1 assuming that all of them lose 25% of their mass after each merger. The masses of the resulting BHs are lower by  $\sim 22 - 28\%$ ; three of the six BHs in Figure 1 are still in the mass gap (tracks 1, 2 and 3), while the remaining three have mass  $< 60 M_{\odot}$ .

Furthermore, the polynomial fitting formulas implemented in MOBSE might be inaccurate to describe the final evolution of such post-merger massive stars. In a follow-up work, we will evolve our post-collision models with a stellar evolution code<sup>1</sup>, to check any deviations from MOBSE. In addition, we assume that the final hydrogen envelope entirely collapses to a BH. This final outcome depends on the final binding energy of the envelope (see e.g. Sukhbold et al. 2016 for a discussion). Finally, we model PPISNe with a fitting formula (Spera & Mapelli 2017) to the models by Woosley (2017). However, the models by Woosley (2017) are suited for stars following regular single stellar evolution, that could be significantly different from merger products.

<sup>1</sup> Glebbeek et al. (2009) re-simulated a runaway collision product with a stellar evolution code. They find that mass loss strongly suppresses the formation of massive mergers at solar metallicity, while a final stellar mass  $\sim 260 M_{\odot}$  is possible at  $Z = 0.001$ . This is similar to our findings. However, their results are not directly comparable with ours, because the original  $N$ -body simulation they start from is composed of 131072 particles; thus, the runaway collision product is significantly more massive than ours.

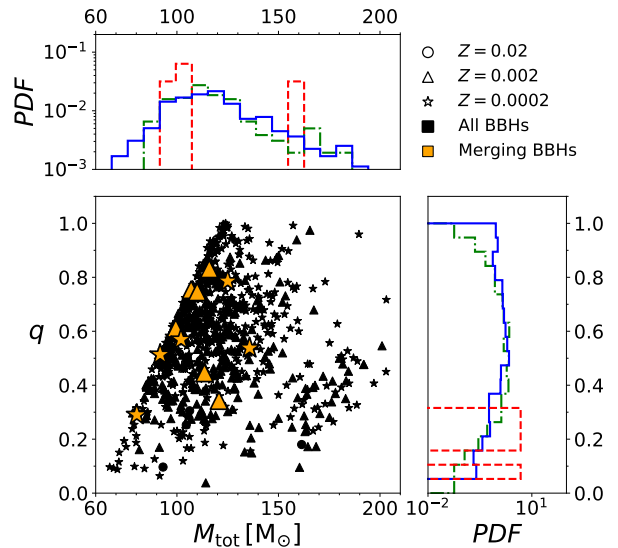


**Figure 2.** Mass ratio  $q = M_2/M_1$  versus total mass  $M_{\text{tot}} = M_1 + M_2$  of BHs with mass in the gap that are members of BBHs by the end of the simulations. Circles, triangles and stars refer to  $Z = 0.02, 0.002$  and  $0.0002$ , respectively. Orange and black symbols refer to BBHs merging within a Hubble time and to all BBHs, respectively. Marginal histograms show the distribution of  $q$  (on the  $y$ -axis) and  $M_{\text{tot}}$  (on the  $x$ -axis). Solid blue, dot-dashed green and dashed red histograms refer to  $Z = 0.0002, 0.002$  and  $0.02$ , respectively.

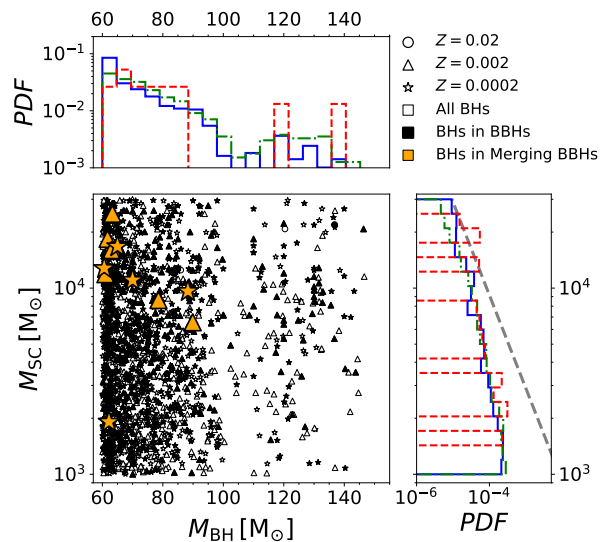


**Figure 3.** Mass of the host star cluster ( $M_{\text{SC}}$ ) versus the mass  $M_{\text{BH}}$  of a BH in the PI gap. Marginal histograms show the distribution of  $M_{\text{SC}}$  (on the  $y$ -axis) and  $M_{\text{BH}}$  (on the  $x$ -axis). Orange and black filled symbols refer to BBHs merging within a Hubble time and to all BBHs, respectively. Open symbols show single BHs. Solid blue, dot-dashed green and dashed red histograms refer to  $Z = 0.0002, 0.002$  and  $0.02$ , respectively. The grey dashed line shows the mass function of  $M_{\text{SC}}$  in our simulation set ( $dN/dM_{\text{SC}} \propto M_{\text{SC}}^{-2}$ ).

**Table 2.** Fraction of BHs, BBHs and merging BBHs with mass in the PI gap.

$Z$	$f_{\text{PI, BHs}}$	$f_{\text{PI, BBHs}}$	$f_{\text{PI, GW}}$	$p_{\text{det}}^{\text{PI}}$
0.0002	$5.6 \pm 0.3 \%$	$20.8 \pm 1.7 \%$	$2.2 \pm 1.9 \%$	11.2 %
0.002	$1.5 \pm 0.1 \%$	$9.6 \pm 1.0 \%$	$2.1 \pm 1.6 \%$	10.0 %
0.02	$0.1 \pm 0.04 \%$	$0.5 \pm 0.5 \%$	0.0 %	0.0 %
S2020	–	–	0.5 %	5.3 %

Column 1 ( $Z$ ): progenitor’s metallicity; S2020 indicates that we accounted for progenitor’s metallicity evolution as a function of redshift, as described in [Santoliquido et al. \(2020\)](#); column 2 ( $f_{\text{PI, BHs}}$ ): percentage of BHs with mass in the PI gap with respect to all simulated BHs at a given  $Z$ ; column 3 ( $f_{\text{PI, BBHs}}$ ): percentage of BBHs that have at least one member with mass in the PI gap with respect to all BBHs at a given  $Z$  formed by the end of the simulations. column 4 ( $f_{\text{PI, GW}}$ ): percentage of merging BBHs that have at least one member with mass in the PI gap with respect to all merging BBHs at a given  $Z$  (a merging BBH is defined as a BBH which merges in less than a Hubble time by GW emission). Errors on  $f_{\text{PI, BHs}}$ ,  $f_{\text{PI, BBHs}}$  and  $f_{\text{PI, GW}}$  correspond to 95% credible intervals on binomial distributions, using a Wald method for approximation. Column 5 ( $p_{\text{det}}^{\text{PI}}$ ): percentage of detectable BBH mergers that have at least one member with mass in the PI gap with respect to all detectable BBH mergers at a given  $Z$  (see equation 3).

### 3.2 Mass distribution

Figure 2 shows the mass ratio  $q = M_2/M_1$  (where  $M_1 > M_2$ ) and the total mass  $M_{\text{tot}} = M_1 + M_2$  of all BBHs that have at least one member in the PI gap. We form BHs with masses in the entire range of the PI gap between  $\sim 60 - 150 M_{\odot}$ , with a preference for masses around  $60 - 70 M_{\odot}$ .

Values of mass ratio  $q \gtrsim 0.4$  are the most likely, but we find binaries with  $q$  as low as  $\sim 0.04$ . The binary with the smallest value of  $q$  has secondary mass  $M_2 \sim 4.2 M_{\odot}$ . The largest secondary mass is  $M_2 \sim 110 M_{\odot}$ . Overall, binaries hosting a BH with mass in the gap have lower mass ratios than other BBHs (see Figure 7 of [Di Carlo et al. 2019](#), where we show that the vast majority of BBHs in young SCs have  $q \sim 0.9 - 1$ ).

Figure 3 shows the mass of the host SC as a function of the mass of BHs in the PI gap (here we include also BHs that remain single). BHs in the mass gap form more efficiently in massive young SCs, where dynamics is more important. Ten out of eleven merging BBHs are hosted in star clusters with  $M_{\text{SC}} > 6000 M_{\odot}$ , among the most massive young SCs in our sample.

### 3.3 Merger and detection efficiency

We find that only  $\sim 0 - 2.2 \%$  of all merging BBHs have at least one member with mass in the PI gap, depending on metallicity. However, these systems are more massive than other merging BBHs, thus they have a higher detection chance. To properly take into account these selection effects, we followed a similar approach as in [Finn & Chernoff \(1993\)](#), [Dominik et al. \(2015\)](#) and [Bouffanais et al. \(2019\)](#).

We associate to each mock source (in our catalogue of 534 merging BBHs) the optimal signal-to-noise ratio (SNR)  $\rho_{\text{opt}}$  that corresponds to the case where the source is opti-

mally oriented and located in the sky. Since real-life sources have different orientations and locations, we then reweigh the SNR as  $\rho = \omega \times \rho_{\text{opt}}$ , where  $\omega$  takes randomly generated values between 0 and 1, and the probability of detecting a source is given by

$$p_{\text{det}} = 1 - F_{\omega}(\rho_{\text{thr}}/\rho_{\text{opt}}). \quad (2)$$

In this equation,  $F_{\omega}$  is the cumulative function of  $\omega$  and  $\rho_{\text{thr}}$  is a detection threshold. We use  $\rho_{\text{thr}} = 8$ , that was shown to be a good approximation for a network of detectors ([Abadie et al. 2010](#); [Abbott et al. 2016c](#)). We used the software PyCBC ([Dal Canton et al. 2014](#); [Usman et al. 2016](#)) to generate both the waveforms (IMRPhenomB with zero spins) and the noise power spectral densities of advanced LIGO at design sensitivity ([Abbott et al. 2018](#)), and the package gwdet ([Gerosa 2019](#)) to evaluate the function  $F_{\omega}$ .

From there, we ran two different analysis: one where each set of metallicity is treated independently, and the other where we combine them together using a model describing redshift and metallicity evolution. In the first scenario, for each metallicity set we construct a catalogue of  $10^6$  sources where the masses are drawn uniformly from the catalogue and redshifts are drawn uniformly in comoving volume between 0 and 1. In the second scenario, we first compute the merger rate at the detector as a function of redshift, by making use of the cosmoRate code ([Santoliquido et al. 2020](#)). In particular, following [Santoliquido et al. \(2020\)](#), we assume that all stars form in young SCs, we account for the cosmic star formation rate ([Madau & Fragos 2017](#)) and for the stellar metallicity evolution ([De Cia et al. 2018](#)), and we take cosmological parameters from [Ade et al. \(2016\)](#). From there, we build a catalogue of  $10^6$  sources, by making use once again of the cosmoRate code ([Santoliquido et al. 2020](#)), to have the distribution of masses as a function of redshift.

Finally, to obtain the probability of detecting a source with at least one component in the PI mass gap, we computed the following quantity for both analyses:

$$p_{\text{det}}^{\text{PI}} = \sum_{i \in \text{PI}} p_{\text{det}}^i / \sum_j p_{\text{det}}^j, \quad (3)$$

where the sum in the numerator is done only over sources where at least one component lies in the mass gap while the sum in the denominator is done over all sources in our catalogue of merging BBHs.

We find  $p_{\text{det}}^{\text{PI}} = 0 - 11\%$ , depending on metallicity (see the last column of Table 2). This means that, under our assumption that all stars form in young SCs, up to 11% of all BBHs detected by LIGO-Virgo at design sensitivity have at least one component in the PI mass gap. If we assume a model-dependent BBH merger rate evolution with redshift (based on the cosmic star formation rate density and on the average metallicity evolution, [Santoliquido et al. 2020](#)), we find  $p_{\text{det}}^{\text{PI}} \sim 5 \%$ , under the assumption that all cosmic star formation takes place in young SCs like the ones we simulated.

## 4 CONCLUSIONS

Pair instability (PI) and pulsational PI prevent the formation of BHs with mass between  $\sim 60$  and  $\sim 150 M_{\odot}$  from

single stellar evolution. However, binary evolution processes (such as stellar mergers) and dynamical processes might allow the formation of BHs with masses in the gap.

Here, we investigate the possibility that BHs with mass in the gap form through stellar mergers and multiple stellar mergers in young SCs. The merger between an evolved star (a giant with a well developed helium core) and a main sequence star can give birth to a BH with mass in the gap, provided that the star collapses before its helium core grows above  $\sim 32 M_{\odot}$ . In our simulations, these stellar mergers are facilitated by the SC environment: dynamical encounters perturb a binary star, affecting its orbital properties and increasing the probability of a merger between its components. Some massive stars even undergo runaway collisions: they go through multiple mergers over few Myrs. When a BH with mass in the PI gap forms in this way, it is initially a single object. If it remains in the SC, it can acquire a new companion through dynamical exchanges. In contrast, BHs that form via stellar mergers in the field remain single BHs. Moreover, BHs with masses  $> 60 M_{\odot}$  are much harder to form in isolated binaries, because non-conservative mass transfer peels-off the primary before the merger. Dynamical encounters perturb the binary and induce a fast merger without episodes of mass transfer.

We have investigated the formation and the dynamical evolution of BHs with masses in the gap through  $10^4$  direct N-body simulations of young SCs with metallicity  $Z = 0.0002, 0.002$  and  $0.02$  and with total mass between  $10^3$  and  $3 \times 10^4 M_{\odot}$ . Hence, we focused on relatively small young SCs. At the end of our simulations,  $\sim 5.6\%$ ,  $\sim 1.5\%$  and  $\sim 0.1\%$  of all BHs have mass in the PI gap for metallicity  $Z = 0.0002, 0.002$  and  $0.02$ , respectively. Metal-poor stars are more efficient in producing these BHs, because they lose less mass by stellar winds. In our simulations, we do not include prescriptions for BH spins, because the connection between the spin of the progenitor star and the spin of the BH is highly uncertain (see e.g. Heger et al. 2005; Lovegrove & Woosley 2013; Belczynski et al. 2017; Qin et al. 2018, 2019; Fuller et al. 2019; Fuller & Ma 2019). We can speculate that stellar mergers spin up the progenitor stars, but we cannot tell whether this spin-up translates into a higher BH spin.

The treatment of the merger of two stars in our simulations is simplified: we assume no mass loss and no chemical mixing during the merger and we require that the merger product reaches hydro-static equilibrium instantaneously. The merger product is rejuvenated according to Hurley et al. (2002) simple prescriptions. Hydro-dynamical simulations of a stellar merger are required in order to have a better understanding of the final outcome. Thus, our results should be regarded as an upper limit to the formation of BHs in the PI mass gap via stellar mergers.

In our simulations, several BHs with masses in the gap end up forming a BBH through dynamical exchanges. BBHs having at least one component in the mass gap are  $\sim 20.6\%$ ,  $\sim 9.8\%$  and  $\sim 0.5\%$  of all BBHs in our simulations, for metallicity  $Z = 0.0002, 0.002$  and  $0.02$ , respectively. Thus, BHs with masses in the gap are quite efficient in forming BBHs. The total masses of these BBHs are typically around  $M_{\text{TOT}} \sim 90 - 130 M_{\odot}$  and the most likely mass ratios are  $q \gtrsim 0.4$ .

In our simulations,  $\sim 2.1\%$  ( $\sim 2.2\%$ ) of all BBHs

merging within a Hubble time have at least one component in the mass gap for metallicity  $Z = 0.002$  ( $Z = 0.0002$ ). We find no merging BBHs in the mass gap at solar metallicity. Merging BBHs in the mass gap form preferentially in the most massive SCs we simulate ( $M_{\text{SC}} \geq 6000 M_{\odot}$ ). Hence, BBH mergers in the mass gap might be even more common in higher mass SCs (e.g. globular clusters) than the ones we simulate. Since merging BBHs in the mass gap form through dynamical exchanges, their spins will be isotropically oriented with respect to the orbital angular momentum of the binary system.

Finally, we calculate the probability that advanced LIGO and Virgo at design sensitivity detect the merger of BBHs in the mass gap. Modelling the dependence of the merger rate on the cosmic star formation rate density and metallicity evolution (Santoliquido et al. 2020), we predict that  $\sim 5\%$  of all BBH mergers detected by LIGO and Virgo at design sensitivity have at least one component in the PI mass gap, under the assumption that all stars form in young SCs. If the proposed mechanism to form BHs in the mass gap is actually at work, the LIGO-Virgo collaboration might be able to witness these events in the next few years.

## ACKNOWLEDGMENTS

We thank the anonymous referee for their useful comments. We thank Mark Gieles, the internal P&P reviewer of the LVC. UNDC acknowledges financial support from Università degli Studi dell'Insubria through a Cycle 33rd PhD grant. MM, YB, NG and FS acknowledge financial support by the European Research Council for the ERC Consolidator grant DEMOBLACK, under contract no. 770017. MS acknowledges funding from the European Union's Horizon 2020 research and innovation programme under the Marie-Sklodowska-Curie grant agreement No. 794393. AB acknowledges support by PRIN MIUR 2017 prot.20173ML3WW 002 "Opening the ALMA window on the cosmic evolution of gas, stars and supermassive black holes". This work benefited from support by the International Space Science Institute (ISSI), Bern, Switzerland, through its International Team programme ref. no. 393 *The Evolution of Rich Stellar Populations & BH Binaries* (2017-18).

## DATA AVAILABILITY

The data underlying this article will be shared on reasonable request to the corresponding authors.

## REFERENCES

- Abadie J., et al., 2010, *Classical and Quantum Gravity*, **27**, 173001
- Abbott B. P., et al., 2016a, *Physical Review X*, **6**, 041015
- Abbott B. P., et al., 2016b, *Phys. Rev. Lett.*, **116**, 061102
- Abbott B. P., et al., 2016c, *Astrophys. J.*, **833**, L1
- Abbott B. P., et al., 2018, *Living Rev. Rel.*, **21**, 3
- Abbott B. P., et al., 2019a, *Physical Review X*, **9**, 031040
- Abbott B. P., et al., 2019b, *ApJ*, **882**, L24
- Ade P. A. R., Aghanim N., Zonca A. e. a., 2016, *A&A*, **594**, A13
- Antonini F., Rasio F. A., 2016, *ApJ*, **831**, 187
- Arca Sedda M., Benacquista M., 2019, *MNRAS*, **482**, 2991

- Arca Sedda M., Mapelli M., Spera M., Benacquista M., Giacobbo N., 2020, arXiv e-prints, [p. arXiv:2003.07409](https://arxiv.org/abs/2003.07409)
- Belczynski K., Bulik T., Fryer C. L., Ruitter A., Valsecchi F., Vink J. S., Hurley J. R., 2010, *ApJ*, **714**, 1217
- Belczynski K., et al., 2016, *A&A*, **594**, A97
- Belczynski K., et al., 2017, arXiv e-prints, [p. arXiv:1706.07053](https://arxiv.org/abs/1706.07053)
- Bouffanais Y., Mapelli M., Gerosa D., Di Carlo U. N., Giacobbo N., Berti E., Baibhav V., 2019, arXiv e-prints, [p. arXiv:1905.11054](https://arxiv.org/abs/1905.11054)
- Carr B. J., Hawking S. W., 1974, *MNRAS*, **168**, 399
- Carr B., Kühnel F., Sandstad M., 2016, *Phys. Rev. D*, **94**, 083504
- Colpi M., Mapelli M., Possenti A., 2003, *ApJ*, **599**, 1260
- Dal Canton T., et al., 2014, *Phys. Rev.*, D90, 082004
- Dale J. E., Davies M. B., 2006, *MNRAS*, **366**, 1424
- De Cia A., Ledoux C., Petitjean P., Savaglio S., 2018, *A&A*, **611**, A76
- Di Carlo U. N., Giacobbo N., Mapelli M., Pasquato M., Spera M., Wang L., Haardt F., 2019, *MNRAS*, **487**, 2947
- Di Carlo U. N., et al., 2020, arXiv e-prints, [p. arXiv:2004.09525](https://arxiv.org/abs/2004.09525)
- Dominik M., et al., 2015, *ApJ*, **806**, 263
- Farmer R., Renzo M., de Mink S. E., Marchant P., Justham S., 2019, arXiv e-prints, [p. arXiv:1910.12874](https://arxiv.org/abs/1910.12874)
- Farr W. M., Sravan N., Cantrell A., Kreidberg L., Bailyn C. D., Mandel I., Kalogera V., 2011, *ApJ*, **741**, 103
- Finn L. S., Chernoff D. F., 1993, *Phys. Rev.*, D47, 2198
- Fryer C. L., Belczynski K., Wiktorowicz G., Dominik M., Kalogera V., Holz D. E., 2012, *ApJ*, **749**, 91
- Fuller J., Ma L., 2019, *ApJ*, **881**, L1
- Fuller J., Piro A. L., Jermyn A. S., 2019, *MNRAS*, **485**, 3661
- Gaburov E., Lombardi Jr. J. C., Portegies Zwart S., 2010, *MNRAS*, **402**, 105
- Gerosa D., 2019, gwdet:Detectability of gravitational-wave signals from compact binary coalescences, [doi:doi.org/10.5281/zenodo.889966](https://doi.org/10.5281/zenodo.889966).
- Gerosa D., Berti E., 2017, *Phys. Rev. D*, **95**, 124046
- Gerosa D., Berti E., 2019, arXiv e-prints, [p. arXiv:1906.05295](https://arxiv.org/abs/1906.05295)
- Giacobbo N., Mapelli M., 2018, *MNRAS*, **480**, 2011
- Giacobbo N., Mapelli M., Spera M., 2018, *MNRAS*, **474**, 2959
- Gieles M., et al., 2018, *MNRAS*, **478**, 2461
- Giersz M., Leigh N., Hypki A., Lützgendorf N., Askar A., 2015, *MNRAS*, **454**, 3150
- Glebbeeck E., Gaburov E., de Mink S. E., Pols O. R., Portegies Zwart S. F., 2009, *A&A*, **497**, 255
- Goodwin S. P., Whitworth A. P., 2004, *A&A*, **413**, 929
- Heger A., Fryer C. L., Woosley S. E., Langer N., Hartmann D. H., 2003, *ApJ*, **591**, 288
- Heger A., Woosley S. E., Spruit H. C., 2005, *ApJ*, **626**, 350
- Hills J. G., Fullerton L. W., 1980, *AJ*, **85**, 1281
- Hurley J. R., Tout C. A., Pols O. R., 2002, *MNRAS*, **329**, 897
- Justham S., Podsiadlowski P., Vink J. S., 2014, *ApJ*, **796**, 121
- Kroupa P., 2001, *MNRAS*, **322**, 231
- Küpfer A. H. W., Maschberger T., Kroupa P., Baumgardt H., 2011, *MNRAS*, **417**, 2300
- Lada C. J., Lada E. A., 2003, *ARA&A*, **41**, 57
- Limongi M., Chieffi A., 2018, *ApJS*, **237**, 13
- Lovegrove E., Woosley S. E., 2013, *ApJ*, **769**, 109
- Madau P., Fragos T., 2017, *ApJ*, **840**, 39
- Mapelli M., 2016, *MNRAS*, **459**, 3432
- Mapelli M., Colpi M., Zampieri L., 2009, *MNRAS*, **395**, L71
- Mapelli M., Ripamonti E., Zampieri L., Colpi M., Bressan A., 2010, *MNRAS*, **408**, 234
- Mapelli M., Zampieri L., Ripamonti E., Bressan A., 2013, *MNRAS*, **429**, 2298
- Mapelli M., Giacobbo N., Ripamonti E., Spera M., 2017, *MNRAS*, **472**, 2422
- Mapelli M., Spera M., Montanari E., Limongi M., Chieffi A., Giacobbo N., Bressan A., Bouffanais Y., 2020, *ApJ*, **888**, 76
- Marchant P., Renzo M., Farmer R., Pappas K. M. W., Taam R. E., de Mink S. E., Kalogera V., 2019, *ApJ*, **882**, 36
- Marks M., Kroupa P., Dabringhausen J., Pawlowski M. S., 2012, *MNRAS*, **422**, 2246
- Miller M. C., Hamilton D. P., 2002, *MNRAS*, **330**, 232
- Özel F., Psaltis D., Narayan R., McClintock J. E., 2010, *ApJ*, **725**, 1918
- Portegies Zwart S. F., McMillan S. L. W., 2002, *ApJ*, **576**, 899
- Portegies Zwart S. F., Baumgardt H., Hut P., Makino J., McMillan S. L. W., 2004, *Nature*, **428**, 724
- Prialnik D., 2000, An Introduction to the Theory of Stellar Structure and Evolution
- Qin Y., Fragos T., Meynet G., Andrews J., Sørensen M., Song H. F., 2018, *A&A*, **616**, A28
- Qin Y., Marchant P., Fragos T., Meynet G., Kalogera V., 2019, *ApJ*, **870**, L18
- Renzo M., Farmer R. J., Justham S., de Mink S. E., Götberg Y., Marchant P., 2020, *MNRAS*, **493**, 4333
- Rodriguez C. L., Zevin M., Amaro-Seoane P., Chatterjee S., Kremer K., Rasio F. A., Ye C. S., 2019, arXiv e-prints, [p. arXiv:1906.10260](https://arxiv.org/abs/1906.10260)
- Sana H., et al., 2012, *Science*, **337**, 444
- Santoliquido F., Mapelli M., Bouffanais Y., Giacobbo N., Di Carlo U. N., Rastello S., Artale M. C., Ballone A., 2020, arXiv e-prints, [p. arXiv:2004.09533](https://arxiv.org/abs/2004.09533)
- Spera M., Mapelli M., 2017, *MNRAS*, **470**, 4739
- Spera M., Mapelli M., Bressan A., 2015, *MNRAS*, **451**, 4086
- Spera M., Mapelli M., Giacobbo N., Trani A. A., Bressan A., Costa G., 2019, *MNRAS*, **485**, 889
- Stevenson S., Sampson M., Powell J., Vigna-Gómez A., Neijssel C. J., Szécsi D., Mandel I., 2019, *ApJ*, **882**, 121
- Sukhbold T., Ertl T., Woosley S. E., Brown J. M., Janka H. T., 2016, *ApJ*, **821**, 38
- Usman S. A., et al., 2016, *Class. Quant. Grav.*, **33**, 215004
- Vigna-Gómez A., Justham S., Mandel I., de Mink S. E., Podsiadlowski P., 2019, *ApJ*, **876**, L29
- Wang L., Spurzem R., Aarseth S., Nitadori K., Berczik P., Kouwenhoven M. B. N., Naab T., 2015, *MNRAS*, **450**, 4070
- Woosley S. E., 2017, *ApJ*, **836**, 244
- Woosley S. E., 2019, *ApJ*, **878**, 49
- Woosley S. E., Blinnikov S., Heger A., 2007, *Nature*, **450**, 390
- Wu S., Everson R. W., Schneider F. R. N., Podsiadlowski P., Ramirez-Ruiz E., 2020, arXiv e-prints, [p. arXiv:2006.01940](https://arxiv.org/abs/2006.01940)